analytical chemistry

Article

pubs.acs.org/ac

# Oil-Isolated Hydrogel Microstructures for Sensitive Bioassays On-Chip

Rathi L. Srinivas, Stephen D. Johnson, and Patrick S. Doyle*

Department of Chemical Engineering, Massachusetts Institute of Technology, Cambridge, Massachusetts 02139, United States

Supporting Information

**ABSTRACT:** Multiplexed, sensitive, and on-chip molecular diagnostic assays are essential in both clinical and research settings. In past work, running reactions in nanoliter- to femtoliter-sized volumes such as microwells or droplets has led to significant increases in detection sensitivities. At the same time, hydrogels have emerged as attractive scaffolds for bioassays due to their nonfouling, flexible, and aqueous properties. In this paper, we combine these concepts and develop a novel platform in which hydrogel compartments are used as individually confined reaction volumes within a fluorinated oil phase. We fabricate functional and versatile hydrogel microstructures in microfluidic channels that are physically isolated from each other using a surfactant-free fluorinated oil phase, generating picoliter- to nanoliter-sized immobilized aqueous reaction compartments that are readily functionalized with biomolecules. In doing so, we achieve monodisperse reaction volumes with an aqueous interior while exploiting the unique chemistry of a hydrogel, which provides a solid and porous binding scaffold for biomolecules and is impenetrable to oil. Furthermore, our lithographically defined reaction volumes are readily customized with respect to geometry and chemistry within the same channel, allowing rational tuning of the confined reaction volume on a post-to-post basis without needing to use surfactants to maintain stability. We design and implement a multiplexed signal amplification assay in which gel-bound enzymes turn over small molecule substrate into fluorescent product in the oil-confined gel compartment, providing significant signal enhancement. Using short (20 min) amplification times, the encapsulation scheme provides up to 2 orders of magnitude boost of signal in nucleic acid detection assays relative to direct labeling and does not suffer from any cross-talk between the posts. We ultimately demonstrate up to 57-fold increase in nucleic acid detection sensitivity compared to a direct labeling scheme.

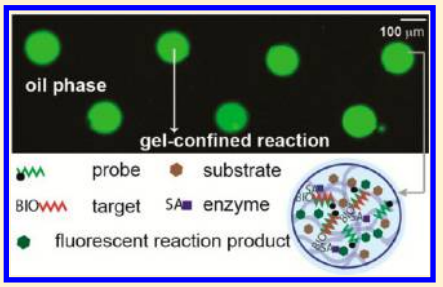


Sensitive biomolecule detection assays with streamlined workflows are crucial for measurement of low-concentration clinical analytes and for precise characterization of biological systems. Many detection strategies employ amplification schemes to achieve sensitivity by labeling surface or bead-bound targets with enzymes that turn over substrate into fluorescent or colorimetric molecules. Since a single target-binding event is reported by the enzymatic turnover of several substrate molecules, the strategy provides signal amplification.[1−4] In standard amplification reactions such as the commercially available enzyme-linked immunosorbent assay (ELISA), these enzyme-assisted amplification reactions occur on microplates with net volumes on the order of 100 μL and are still considered the gold standard for protein detection. Recent studies have, however, been successful in further amplifying net signal and gaining up to 3 orders of magnitude increase in assay sensitivity by shrinking the reaction volume to concentrate the reaction products.[5−11] By examining thousands of reaction volumes, some of these assays have digitized signal output at the lower end of their calibration curves, enabling single-molecule detection of target-enzyme complexes.

To this end, researchers have explored a number of platforms for the creation and utilization of stable and monodisperse miniature reaction compartments. For example, femtoliter-sized microwells, which are large enough to hold a single 3−5 μm diameter bead, have been fabricated using etched optical-fiber bundles or injection molding of polymers.[5−7,12] In other systems, similarly sized bead-filled droplets have been arrayed on hydrophobic surfaces patterned with hydrophilic wells.[8,9] Individual beads with target-enzyme complexes and the enzymatic substrate solution are then confined into the compartments and sealed using mechanical force or, in more recent work, inert fluorinated oil.[5,7,9] Meanwhile, slightly larger (picoliter to nanoliter) sized microwells and surfactant-stabilized droplets have been made using soft lithography and microfluidic techniques.[10,11,13−19] In all of these platforms, the confined reaction volume provides significant increases in reaction sensitivity in comparison to reactions run in bulk.

It is apparent that both microwells and droplets have favorable characteristics applicable to carrying out biological assays. While microwells are physically immobilized and have well-defined boundaries dictated by the fabrication process, droplets provide a naturally aqueous environment to foster biological reactions. However, water droplets require introduction of a solid substrate (e.g., microsphere) if they are to be functionalized with biological moieties such as nucleic acids. Furthermore, liquid manipulation in and out of microwells and

**Received:** October 4, 2013
**Accepted:** November 15, 2013
**Published:** November 15, 2013

   dx.doi.org/10.1021/ac403201p | Anal. Chem. 2013, 85, 12099−12107

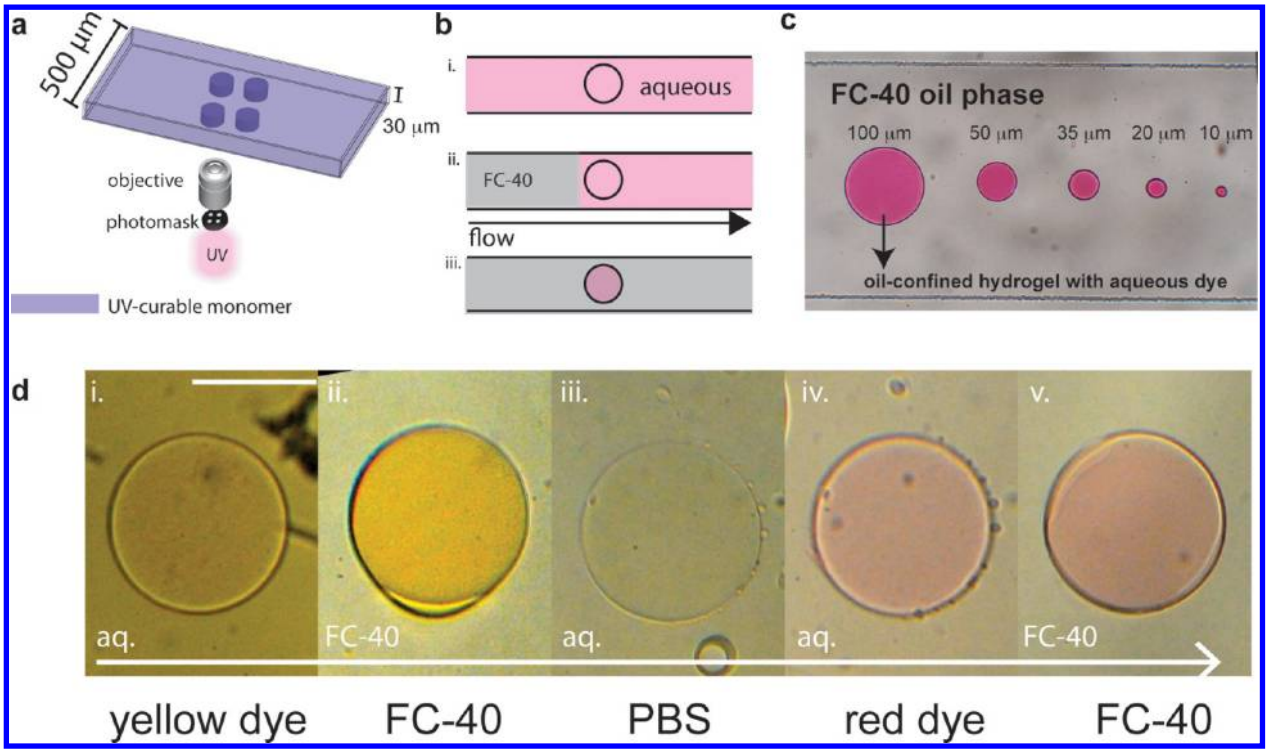


**Figure 1.** Hydrogel post polymerization and oil-isolation. (a) Gel posts are polymerized using projection lithography. The channel is filled with monomer solution, and then photomask-patterned UV light is projected through a microscope objective. Posts adhere covalently to the TPM-modified channel. (b) Solutions are flushed in and out of the post-bearing channel: (i) the channel is filled with an aqueous solution containing assay reagents which diffuse into the gel, (ii) the aqueous phase is replaced using a flush with FC-40 oil, forming a 2-phase flow in the device, and (iii) the oil conformally coats the gel post, enabling retention of any reagents inside the volume of the gel. The gel post is now completely isolated. (c) Isolated compartments of different size are created on the same microfluidic chip. In this example, each isolated compartment retains a volume of aqueous food dye proportional to the gel post volume. (d) Using a straight microfluidic channel interfaced with a pressure-driven flow allows easy exchange of reagents in and out of the device. In this example, a channel is initially filled with an aqueous solute (yellow food dye), and the solute-loaded gel is then confined with an oil-flush. The channel is rinsed with an aqueous buffer to release the contents of the gel, and reloaded with a new aqueous solute (red food dye). The process is repeated. Scale bar is 100 $\mu$m.

droplets can be challenging and often requires intricate fluidics.[11] Thus, a platform that incorporates the favorable characteristics of microwells and droplets while providing more flexibility in terms of biological functionalization and reagent exchange would be of high value.

One can envision an immobilized hydrogel mesh as a hybrid between a microwell and a droplet in terms of its potential ability to act as a solid yet aqueous compartment for reactions. Lithographic techniques can be used to photopattern hydrogel microstructures with photomask-defined shapes and sizes into channels.[20−22] It is additionally straightforward to covalently functionalize a hydrogel mesh with biological probes or other functional groups at the time of polymerization. The resulting compartment itself is chemically unique, since it serves as both an immobilized aqueous reaction volume and as a fully functional mesh for physical or chemical entrapment and reaction of biological species.

Hydrogel microstructures have been previously implemented for microfluidic flow control,[23] biomolecular detection,[21,24−32] and cell encapsulation/patterning.[21,22] In addition, a series of recent studies has used submicroliter hydrogel posts as individual PCR reaction chambers.[33−35] From a biological standpoint, many of the aforementioned studies have shown that the nonfouling, flexible, and solution-like nature of a hydrogel mesh renders it superior to rigid surfaces for nucleic acid capture and for immobilization of biological probe molecules.[24−26,36] Furthermore, chemical characteristics of the gel, such as porosity, can be fine-tuned by adjusting the starting monomer composition.[37]

In this study, we photopattern porosity-tuned polyethylene glycol (PEG) hydrogel posts into microfluidic channels using projection lithography (Figure 1a) and demonstrate their use as isolated picoliter−nanoliter sized reaction compartments within a surfactant-free fluorinated oil phase. Using pressure-driven fluidics, reagents are easily exchanged in and out of the device. The porosity of the gel is tuned such that solutes introduced in the aqueous-phase will rapidly load into the gel post via diffusion (Figure 1b.i) The hydrodynamic resistance in the gel relative to that of the channel ensures that effects of convection are negligible in the gel (see Supporting Information (SI)). The subsequent introduction of a water-immiscible fluorinated oil phase into the device leads to the aqueous phase being swept out of the channel (Figure 1b.ii). In the process, since the oil cannot penetrate the pores of the hydrogel, it instead conformally coats the gel post, effectively sealing off its contents. Since there is no convective transport through the pores of the gel, the reagents inside the gel are not swept out upon introduction of the oil (Figure 1b.iii). At the end of the process, what remains is an oil-isolated hydrogel post that can act as a confined reaction compartment.

By simply changing the photomask, monomer composition, or UV exposure-time (even within the same channel), we have precise control over post geometry and chemistry for a range of applications, which is one unique feature of the system shown


dx.doi.org/10.1021/ac403201p | Anal. Chem. 2013, 85, 12099−12107

here. The post geometry accordingly dictates the volume of the isolated gel compartment when an oil phase is later flushed through the channel. An example of this control is seen in Figure 1c, where hydrogel posts of different size (10−100 $\mu$m diameter) were polymerized in tandem in the same microfluidic channel. The device was filled with an aqueous food dye, which initially diffused everywhere in the channel and into the gel posts. The FC-40 oil flush then replaced the aqueous phase in the device and conformally coated the gel posts, creating post-size dependent isolated compartments that retained the food dye. The small pore sizes and hydrophilic nature of the gel ensure that the aqueous material within the gel matrix is not displaced by the oil phase. Additionally, by replacing the oil phase in the channel with a different aqueous phase containing a new solute, the gel post can be reloaded and once more reconfined, allowing for easy loading and unloading (Figure 1d).

We apply this novel concept of oil-encapsulation of a hydrogel to design a confined-volume enzymatic amplification reaction which occurs entirely on-chip. Porosity-adjusted gel posts are fabricated with covalently embedded biological probes. Based on prior work from our group, the pore size is tuned such that large (>500 KDa) biomolecules can diffuse and react freely through the gel matrix.[37,38] We use a biotinylated probe to characterize the system and to design the enzymatic assay workflow. We show that the oil-flush is crucial for signal retention inside the gel and that there is no appreciable post-to-post cross-talk. Finally, we design a multiplexed nucleic acid assay in which DNA probes embedded in the hydrogel posts are hybridized with the complementary target, labeled with enzyme, loaded with a small molecule substrate in an aqueous phase, and immediately isolated using oil, allowing the amplification reaction to occur in a physically confined aqueous gel compartment within the oil phase. The resulting product molecules are insoluble in the oil and instead accumulate in the isolated hydrogel post volume. The confined volume therefore allows for increase in effective concentration of the fluorescent small molecule product, leading to almost 2 orders of magnitude boost in net signal with short (20 min) amplification times relative to a direct labeling scheme at low (10 pM) target concentrations. We achieve up to 57-fold increase in limit of detections and observe a linear response over 2.5 logs using the platform.

## MATERIALS AND METHODS

**Device Fabrication and Surface Activation.** Straight PDMS (Sylgard) microchannels were fabricated using soft lithography. Channel inlets and outlets were punched using a 15-gauge Luer stub, and channels were sonicated in ethanol and dried with argon gas prior to use. Glass slides (VWR, 24 mm × 60 mm) were soaked for 1 h in a 1 M NaOH bath, rinsed with DI water, and dried using argon gas. The PDMS channels and glass slides were plasma-treated (Harrick) on medium RF for 25 s, bonded together, and heated at 80 °C for 20 min. In order to ensure adhesion of hydrogel posts to the glass, channels were then treated with 2% (v/v) solution of methacryloxypropyl trimethoxysilane (Sigma, TPM). The TPM solution was prepared in 25% (v/v) PBS in ethanol with pH adjusted to 5. The channels were then rinsed and sonicated in ethanol, and cured at 80 °C for 20 min. Before usage, devices were once more rinsed and sonicated in ethanol.

**Hydrogel Post Polymerization.** A photomask with desired post shape was placed in the field-stop of an inverted microscope (Zeiss Axio Observer A1). The device was filled with monomer solution using a pipet and aligned on the microscope stage using a CCD (Andor Clara). Posts used for bioassays were UV-polymerized for 85 ms through a 20× microscope objective (Zeiss Plan-Neofluar, NA = 0.5). Exposure time was controlled using an external shutter (Sutter). After each round of polymerization, the channel was rinsed using 1× PBS and filled with the subsequent monomer solution. Biological probes were purchased from IDT with an acrydite modification to allow covalent copolymerization into the gel. See SI for additional details on monomer compositions and probes (SI Table S1).

**Assay Workflow.** Prior to running bioassays, channels were filled with a 3% (v/v) solution of Pluronic F-108 (Sigma) in nuclease-free water (Affymetrix) for 1 h to block the glass and the gel posts. Streptavidin-$\beta$-galactosidase (SAB) was diluted in PBS with 0.2% (v/v) Tween-20 (PBST) and filtered through a 0.2 $\mu$m syringe filter prior to use. All DNA targets were diluted in 1× PBS. All incubations occurred under a 1 psi pressure-driven flow at a final flow-rate of 10 $\mu$L/min. A 1 mL syringe (BD) with the plunger removed was connected to tygon tubing, which was then connected to house air through a pressure gauge (0.2−25 psi outlet range, Controlair, Inc.). After each incubation step, the channel was rinsed using a 300 $\mu$L volume of PBST. The final two steps of the enzymatic reaction were done using a hand-held 1 mL syringe fitted with a cut 200 $\mu$L pipet tip on the end. Fluorescein-di-$\beta$-galactopyranoside (FDG) was always diluted into PBST to a final concentration of 200 $\mu$M and flowed through the device for 15 s. This was immediately followed by a 10 s flush with fluorinated oil (FC-40, Sigma). All imaging was done using fluorescence or bright field microscopy using a 10× objective (Zeiss Plan-Neofluar, NA = 0.3). Images were analyzed by averaging signal over the post area.

## RESULTS AND DISCUSSION

**Assay Development.** All biological studies were done using cylindrical posts with a radius of 75 $\mu$m prepared using PEG-diacrylate based monomer solutions that were developed and optimized by our group for multistep hydrogel-based bioassays requiring reaction and diffusion of large (>500 KDa) biomolecules.[37−40] It is possible to tune the pore size of the mesh by changing the relative concentrations of the active cross-linking species (PEG-diacrylate), the photoinitiator, and the porogen (PEG-200 or PEG-600). Porogens with larger molecular weights lead to gel networks with higher average porosity without reducing functionalization of biological molecules into the matrix.[37] The monomer mixture used here (see SI) gave our gels a mesh size of up to hundreds of nanometers.[37] The monomer chemistry also dictates the functionalization efficiency of acrylate-modified biological species. Gels that are more tightly cross-linked will incorporate higher concentrations of biological probes but will also have smaller pore sizes and will lead to reduced diffusion through the gel, leading to a trade-off. The chemistry we use here leads to the incorporation of acrylate-bearing nucleic acid probes into the hydrogel matrix with an efficiency of ∼10% under the described synthesis conditions.[37,38] By simply exchanging the monomer in the device after each round of synthesis, posts bearing different biological functionalities (e.g., DNA sequences) could be polymerized within the same device. We chose to use straight microfluidic channels to enable a streamlined workflow with respect to reagent exchange through the device,


dx.doi.org/10.1021/ac403201p | Anal. Chem. 2013, 85, 12099−12107

although our workflow would be amenable with a wide range of microfluidic geometries. Here, we were able to interface the chip with a pressure-controlled flow system as described in previous work.[41]

We first optimized reagent delivery and target incubation conditions using immobilized gel posts functionalized with biotinylated DNA for facile attachment of streptavidin-conjugated species as shown in Figure 2a. Analytes were delivered in a flow-through format where it is important to eliminate any mass-transfer limitation imposed by the delivery rate of the analyte to the surface of the gel posts. By using a high Péclet number (Pe > 1E4, see SI for explanation) flow in the device, we ensured that the analyte concentration at the surface of the post would constantly be equivalent to the bulk concentration, making any resulting depletion zone negligible. We further considered the potential diffusional limitation imposed by the hydrogel network. Biological species such as nucleic acids and proteins diffusing and reacting within similar gel networks have a high (>50) Dahmköhler number, often leading to a reaction boundary layer around the gel.[38] However, given enough time, the target will diffuse into and react with all parts of a porosity-adjusted gel. In previous work with hydrogel particles, we have found that biotin-streptavidin reactions approach equilibrium in 45−60 min. We sought to achieve similar reaction times using the gel posts.[40] We characterized the assay using 2 ng/$\mu$L streptavidin-phycoerythrin (SA-PE, Life Technologies), a 300 KDa fluorophore. By imaging progression of the reaction under flow over 60 min, we first verified that there was no formation of depletion zones around the gel posts and that the gel did not interact significantly with the fluorophore. We further observed diffusion and reaction of the fluorophore into the gel over time until the gel was saturated with the fluorophore (Figure 2b). As expected, the outermost section of the gel saturates first, but over the time

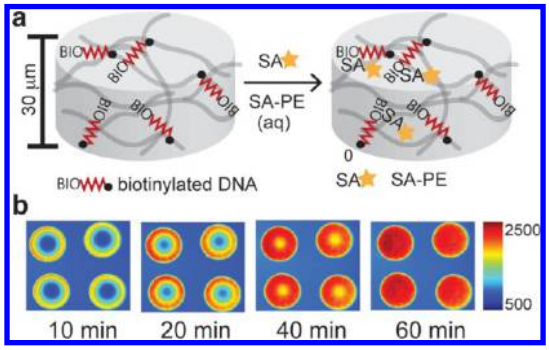


**Figure 2.** (a) Simplified workflow in which gel posts functionalized with biotinylated DNA are incubated with streptavidin phycoerythrin. (b) Signal collection in posts over 60 min showing that fluorophore diffuses and reacts throughout the gel under the provided analyte flow conditions.

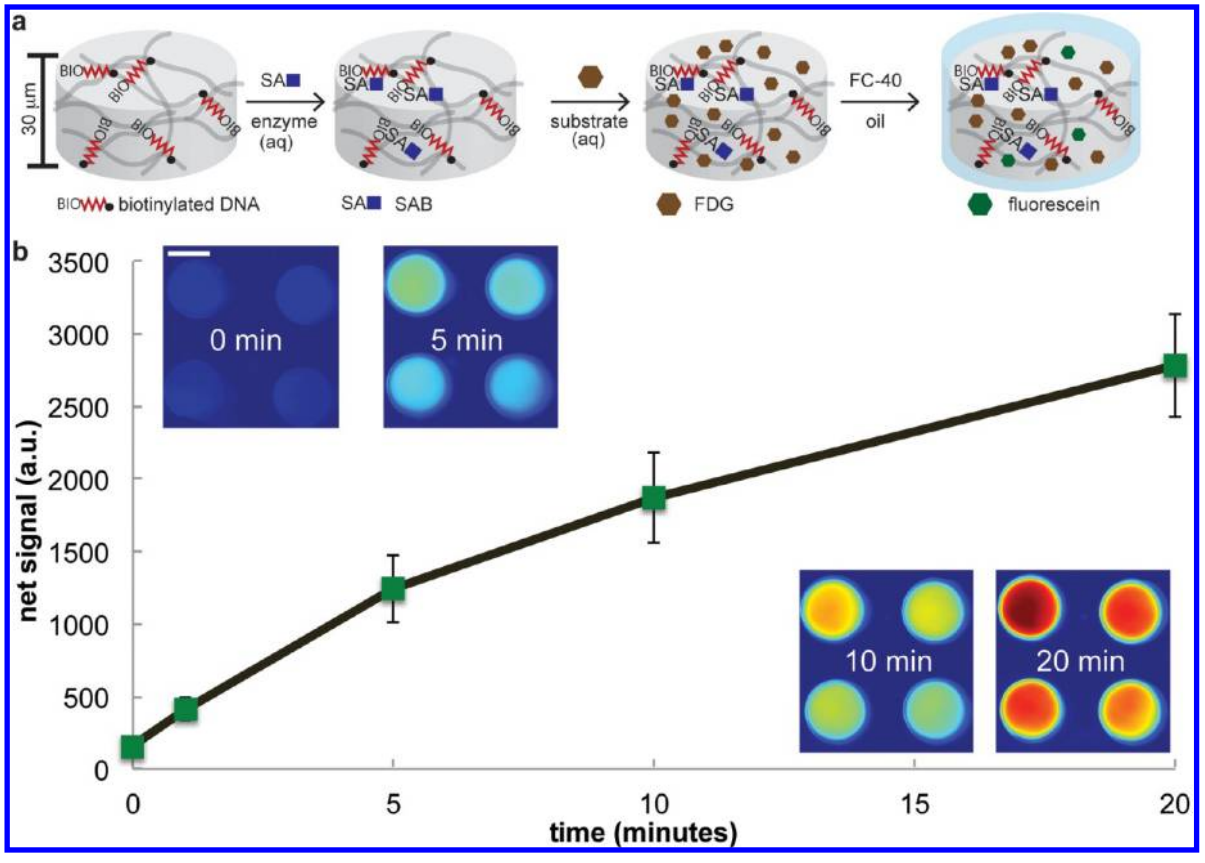


**Figure 3.** Enzymatic amplification scheme. (a) Gel posts are polymerized with biotinylated DNA. Mesh size is optimized to allow diffusion of biomolecules in and out of the matrix. The posts are reacted with a streptavidin-conjugated enzyme (SAB) and then loaded with the enzymatic substrate (FDG). In the final step, the posts are isolated within a fluorinated oil phase, ensuring that fluorescent reaction products are confined within the gel compartment. (b) Time-lapse data showing generation of signal within the gel posts after the oil isolation, and heat-mapped images showing signal progression over time. Over 20 min, the posts generate 17-fold signal relative to starting background signal. Scale bar in images is 100 $\mu$m.


dx.doi.org/10.1021/ac403201p | *Anal. Chem.* 2013, 85, 12099−12107

course of 60 min, we observed reaction throughout the entire gel. Furthermore, we only observed fluorophore binding on biotin-functionalized posts (SI Figure S1). Because of a high Pe flow in the channel, the directionality of the flow does not impact the way that the gel post saturates with signal, since all surfaces of the post are in contact with bulk concentration of the target at all times. The channel was then rinsed using PBST for evaluation of the posts at the conclusion of the assay. We assessed post-to-post monodispersity and uniformity of functionalization after labeling. All of our posts remained the same size (radius of 75 $\mu$m) after the assay, and we calculated <5% coefficient-of-variation in fluorescence signal from post-to-post (SI Table S2). These initial assays thus allowed us to characterize the fundamental aspects of our system and to also optimize parameters such as flow-rates and incubation times.

The confined enzymatic amplification assay was then designed using the aforementioned biotinylated gel posts and streptavidin-conjugated enzymes. Our final workflow is shown in Figure 3a, which depicts the reaction that occurs on a single post inside the channel. We carried out the enzyme incubations using the flow conditions that we had previously optimized using SA-PE. The streptavidin-conjugated enzyme was first flowed through the device for 1 h at a flow-rate of 10 $\mu$L/min followed by a PBST rinse step to remove any unbound enzyme. The device was then loaded with the small molecule enzymatic substrate solution, which rapidly diffused into the hydrogel posts. Once turned over by the enzyme, this small molecule substrate became fluorescent.

It is important to note that the addition of the substrate is fundamentally different from prior steps of the assay. While these prior steps render biomolecules such as the streptavidin-conjugated enzyme physically bound to the biotinylated gel scaffold, it is not possible to physically entrap the rapidly diffusing enzymatic substrate molecules in the mesoporous gel scaffold due to their smaller size. While the gel pore size is on the order of hundreds of nanometers, the small molecules have radii on the order of angstroms. However, when the aqueous phase is displaced using FC-40, the oil conformally coats the gel post, physically retaining any substrate molecules present in the compartment, as we had also previously observed with the aqueous food dyes (Figure 1c). We also noticed that there might be some chemical tendency of the hydrophobic small molecule substrate to partition into the gel matrix, providing a locally higher concentration of the substrate in the gel posts relative to the surrounding channel immediately prior to the oil flush (SI Figure S2), but it is unclear how much this impacts the assay. In future studies, it may be possible to alter the gel chemistry to leverage these partitioning effects. Once the gel volume is isolated, the enzymatic reaction continues in the confined compartment, leading to amplification of signal as the reaction product concentration increases.

A crucial design challenge in the described workflow is to ensure that the enzymatic reaction does not proceed substantially in the time that it takes to replace the aqueous substrate-containing phase with the fluorinated oil phase. Otherwise, these reaction products may be lost to convection and/or may diffuse into other posts, introducing post-to-post cross-talk. Preventing these problems required careful choice of an enzyme/substrate pair. When considering potential enzymes, we first ruled out horseradish peroxidase (HRP) due to its need for multiple substrates, which would complicate the proposed workflow. Additionally, one of these substrates, $H_2O_2$, is unstable once diluted. Finally, other researchers that have investigated HRP for use in femtoliter-sized wells have found that the turnover rate decreases up to 10-fold in confined settings and that the enzyme can be allosterically inhibited by its product.[42,43] Similar to other confined reaction platforms, we chose to use streptavidin-B-galactosidase (SAB, Life Technologies), an enzyme compatible with several different small molecule substrates that follow standard Michaelis–Menten kinetics even in confined situations.[6]

Resorufin-B-galactopyranoside (RGB, Life Technologies) and fluorescein-di-B-galactopyranoside (FDG, Life Technologies) were both considered as potential substrates. Although RGB is known to have a faster turnover rate than FDG, proceeds via single-step catalysis, and has been successfully used in the digital ELISA assay, we noticed that the reaction generated significant fluorescent product before the oil encapsulation step at high gel-bound enzyme concentrations. We also found that the starting material had high fluorescence background. We expect that the difference between the digital ELISA and our assay can be explained by effective enzyme concentration at the start of the reaction in the two different platforms. In the digital ELISA assay, beads are typically labeled with no more than 1–10 enzyme molecules, likely making the initial turnover rate slower, especially in bulk (100 $\mu$L) before the microwell confinement.[6,44] In contrast, if we assume even a 50% enzyme capture efficiency rate in the gel over a 1 h enzyme incubation based on time-scales derived in our previous work,[38] at high (>50 nM) gel-bound biotin concentrations, we would still be binding >$10^6$ enzyme molecules over the volume of the gel (100 pL). The hydrogels thus have a locally higher enzyme concentration relative to enzyme-labeled beads in a bulk solution (100 $\mu$L), which leads to faster initial substrate turnover rates.

The FDG substrate has also been successfully used in droplet-based digital ELISA approaches, but its turnover mechanism is different from that of RGB. It is converted through a two-step reaction in which the first step is rate-limiting, leading to a delay in generation of fluorescent product while the intermediate substrate for the second step of the reaction builds up.[45] This natural delay could provide enough time to oil-confine the posts before generation of measurable reaction product. We tested this hypothesis in a proof-of-concept assay by reacting 50 pg/$\mu$L of SAB with gel posts containing high concentration of biotinylated DNA probe (500 nM) for 1 h and following with FDG (200 $\mu$M) and FC-40. The posts were then time-lapse imaged under fluorescence for 20 min (Figure 3b). When analyzing the posts, we chose to use the mean signal from the entire circular area of the post. Line scans across the diameter of the post show similar fluorescence profiles across the top, middle, and bottom of the posts (SI Figure S3). The progression of the signal is seen in Figure 3b, where, even 1 min after encapsulation, there is only a 2.6-fold increase in signal from the posts relative to initial background. This suggested that the reaction did not generate quantifiable reaction product until significantly after the oil isolation of the posts. In contrast, after 20 min, we measured a 17-fold increase in net signal in the posts relative to our starting time, and noted that the signal had gradually grown over time. The growth of signal over time ensured that our confined enzymatic scheme allowed collection of fluorescent small molecules inside the posts.

Based on these initial results, we ran all other reactions for the same time course, reasoning that while this was enough time to generate measurable signal, it would also allow us to

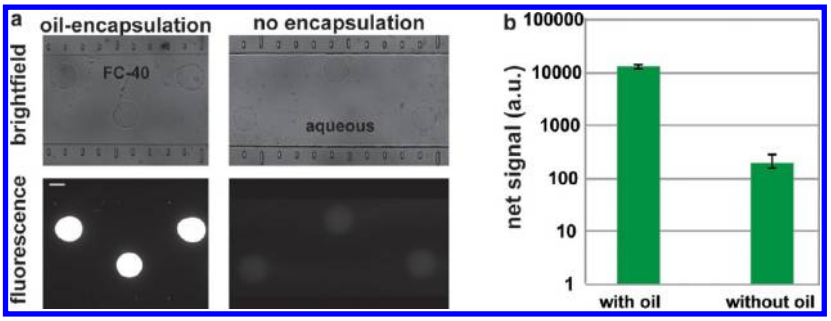


**Figure 4.** (a) Bright-field and fluorescence images comparing signal within the gel posts after enzymatic amplification both with and without oil encapsulation. In the former case, there is significantly more signal retained inside the gels and no diffusion of product into the channel. Scale bar is 100 $\mu$m. (b) Quantitative analysis showing that the encapsulation step provides over 60-fold increase in net signal relative to simply running the reaction in an aqueous phase.

maintain a reasonable assay dynamic range. By running the reaction for longer times, we could generate more signal but would also risk saturating the detection sensor. The concentration of SAB was increased 2-fold for all subsequent reactions to increase enzyme kinetics in the final step of the amplification. We also noticed that gel posts in close proximity sometimes led to isolation of multiple posts in one volume or led to the formation of water channels between posts. In all ensuing assays, we chose to orient the posts in a staggered position to provide sufficient (at least 300 $\mu$m) lateral distance between posts such that each post would be separately isolated by the oil phase. Changing the size of the post or the flow-rate of oil could also be explored to ensure robust isolation.

**System Characterization.** Since previous studies have used PEG hydrogel substrates in the aqueous phase without confinement to design enzymatic assays for glucose sensing, we sought to first quantify any signal enhancement gained by using the final oil-isolation step for our hydrogels. There are two main differences between the gels shown here and those used in prior studies.[27,28,46] First, gels in other studies are typically more cross-linked due to longer UV-exposure times and different monomer compositions. Second, the prior studies physically entrap the enzyme into the matrix upon polymerization. Since the only species that must diffuse into the gel are small molecules such as glucose and the enzymatic substrate, the pore size of the gel is not as crucial.

In contrast, our gel network is chemically and structurally different in that it is designed to undergo a multistep bioassay requiring both diffusion and reaction of large species. It was thus important to understand the advantage gained by encapsulating the gel using oil in the final step relative to simply allowing the enzymatic reaction to occur without the isolation. To this end, two identical devices were each prepared with two kinds of posts: biotinylated posts containing a final concentration of 50 nM biotinylated DNA and "blank" posts containing no biotin as a control. The control allowed us to calculate the net background-subtracted signal arising from the biotinylated posts. We flowed 100 pg/$\mu$L of SAB through each device for 1 h and rinsed out excess enzyme using PBST. Both devices were then flushed with FDG, but only one device was subject to the final FC-40 flush. After 20 min, both devices were imaged for fluorescence signal from posts (Figure 4a) First, we noticed that although the hydrogel posts were able to naturally retain some fluorescent product without being oil-encapsulated, there was rapid diffusion of the product into the channel (SI Figure S4), which would certainly contribute to cross-talk in a multiplexed setting and would decrease assay sensitivity. Second, even though there was measurable background-subtracted signal from these nonconfined posts, it was far less than the net signal we observed when the posts were oil-encapsulated. We measured at least a 60-fold net signal increase due to the oil-isolation (Figure 4b) While the actual enhancement may have been greater, our detector was saturated at this high biotin concentration.

Our next task was to evaluate any cross-talk generated in the channel as a result of the substrate and oil flush steps by designing an experiment to quantify the effect of high signal-generating biotinylated posts on the signal recorded from adjacent control "blank" posts in the same channel. In an "intrachannel" scenario, both biotinylated posts (5 nM) and control posts were immobilized in the same channel. In an "interchannel" scenario, biotinylated posts and control posts were immobilized in separate channels. SAB, FDG, and FC-40 were then flowed through all three channels and posts were imaged after 20 min. We mimicked the scenario most likely to generate cross-talk: a situation in which high-signal-generating posts upstream of the control may prematurely begin to react and generate fluorescent product, which is then swept downstream into the control posts before encapsulation. All reagents were accordingly flowed from the side of the channel containing the biotinylated posts toward the side of the channel containing the control posts in the intraplex assay (Figure 5a). Comparison of the fluorescence signals from the intraplex assay and interplex assay showed that the baseline subtracted signal was the same for both biotinylated and control posts in both situations, ensuring that the assay workflow did not cause any measurable cross-talk (Figure 5b).

**Multiplexed Nucleic Acid Assay.** Since there was negligible cross-talk between posts, it was possible to run multiplexed assays within the same device. We implemented an intrachannel multiplexed nucleic acid detection assay using a set of three short (20 nucleotide) DNA probe sequences (see SI Table S1) and corresponding complementary biotinylated targets which would not cross-react with each other based on prior work with nucleic acid capture on hydrogels.[38,47,48] Posts containing 10 $\mu$M DNA probe 1, 10 $\mu$M DNA probe 2, and 10 $\mu$M DNA probe 3 were polymerized adjacent to each other in the same microfluidic channel (Figure 6a). The workflow was slightly modified to accommodate an additional incubation step in which biotinylated targets would hybridize with the gel-embedded probes. In this target flow step, channels were initially either incubated with 0 pM of all DNA targets or with 10 pM of all DNA targets diluted in 1× PBS (140 mM NaCl) for 1 h at room temperature. After rinsing with PBST, posts

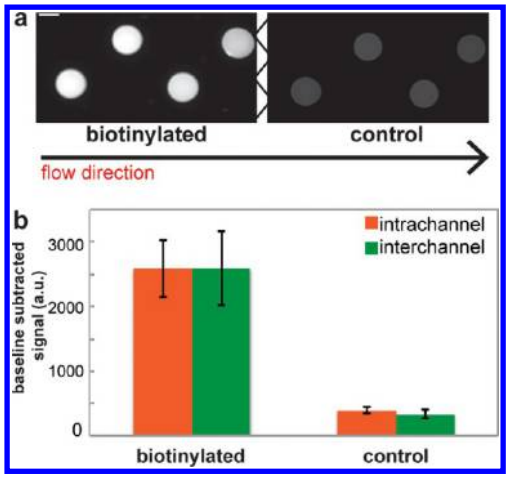


**Figure 5.** (a) Fluorescence images showing results from an intraplex assay in which biotinylated and control posts are immobilized in the same channel. Reagent flow goes from high-signal generating biotinylated posts toward control posts. Scale bar is 100 $\mu$m. (b) Quantitative analysis of data from intraplex and interplex assays demonstrating no significant cross-talk as a result of substrate or oil flush steps.

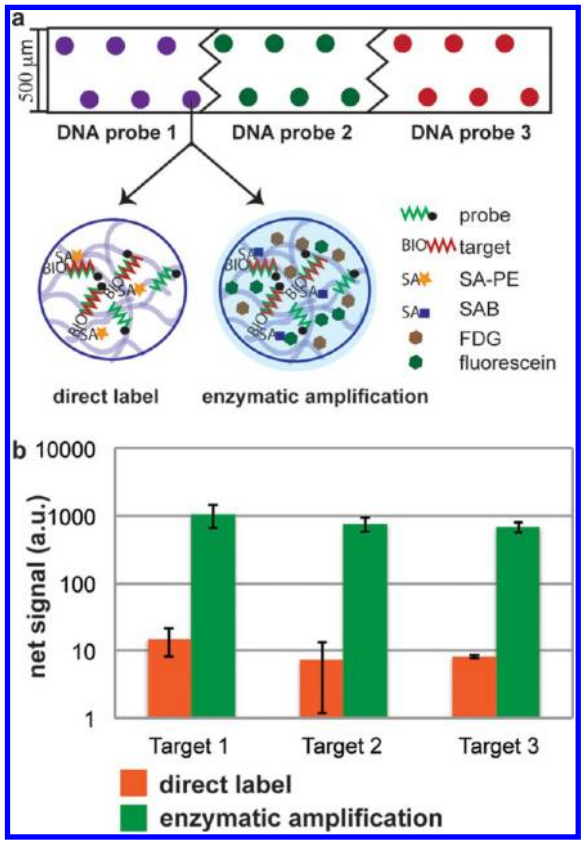


**Figure 6.** Multiplexed DNA assay workflow. (a) Posts functionalized with probes against different sequences are polymerized adjacent to each other in the same channel. After incubation with the biotinylated target sequences, the posts are labeled either using SA-PE or using SAB. The latter posts are then loaded with substrate and isolated for the amplification reaction. (b) A sample incubation with 10 pM target showing 70−100-fold increase in net signal of the enzymatic scheme (after 20 min of amplification) in comparison to direct labeling.

were directly labeled using either 2 ng/$\mu$L of SA-PE or 100 pg/$\mu$L of SAB for 1 h. The latter channels were finally flushed with FDG and FC-40. This allowed us to compare the boost in signal from the 20 min amplification step relative to our most robust direct labeling scheme at low concentrations of DNA target.[40] In this case, the signal arising from the 0 pM target channels was considered the "control", and net signal was computed by subtracting the signal arising from posts in these channels. We chose 10 pM as a "low" DNA target concentration based on previous studies that have captured and directly labeled similarly sized nucleic acid sequences on hydrogel substrates.[47,21,47] In these prior studies, 10 pM DNA target is either close to the limit of detection or out of the detection range.[21,48] Accordingly, for all three targets, we observed a barely detectable net signal at 10 pM target from the direct labeling scheme using SA-PE. In contrast, there was almost 2 orders of magnitude increase in net signal using the encapsulated enzymatic amplification for just 20 min (Figure 6b).

The next goal was to ascertain the sensitivity of our new assay and compare it to what would be achievable through the direct labeling scheme with SA-PE. We prepared posts in a series of channels in order to generate a dose−response curve for both schemes (direct label versus enzymatic amplification). Target concentrations were evaluated across the same range for both schemes. DNA targets were diluted at concentrations ranging from 500 fM to 500 pM in 1X PBS. The same protocol mentioned previously was followed for each target concentration.

The calibration curves are shown in Figure 7, and resulting limits of detection are tabulated in Table 1. Limit of detection

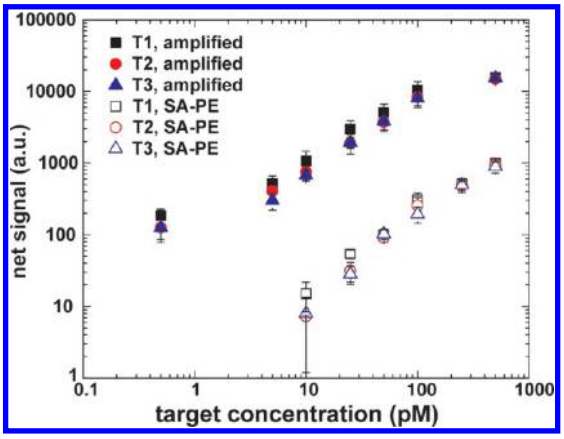


**Figure 7.** Calibration curves showing signal versus target concentration for three nucleic acid targets using both SA-PE (open symbols) and the enzymatic amplification (closed symbols).

was defined here as the target concentration at which the signal-to-noise ratio is 3. We took the assay noise to be the standard deviation calculated from the 0 pM target incubation.

**Table 1. Tabulated LODs for Direct Labeling Scheme and for Enzymatic Amplification Scheme**

| | LOD SA-PE (pM) | LOD enzymatic amplification (pM) | fold-increase in sensitivity |
|---|---|---|---|
| DNA target 1 | 8.2 | 0.37 | 22 |
| DNA target 2 | 13 | 0.23 | 57 |
| DNA target 3 | 10 | 0.40 | 25 |


dx.doi.org/10.1021/ac403201p | Anal. Chem. 2013, 85, 12099−12107

There was 22−57-fold improvement in assay sensitivity depending on the nucleic acid sequence when using the enzymatic amplification. Furthermore, we noted a linear response from 500 fM to 100 pM for the enzymatic amplification and from 25 pM to 500 pM for the direct labeling. In the case of the amplification reaction, the curve hits saturation due to the exposure time of our camera and not because of intrinsic reaction saturation. By changing the imaging conditions, it should be possible to gain linearity over a longer range. In future assays, we could change post sizes, arraying strategy, or channel dimension to increase the number of targets that can be multiplexed.

## CONCLUSIONS

In this Article, we have shown the development and application of a novel multiplexed platform that provides a facile route to generating isolated hydrogel compartments within a fluorinated oil phase. We applied this concept to boost the signal in DNA detection by retaining enzymatic reaction products within gel compartments. The concept of encapsulating hydrogel compartments using oil offers many further possibilities due to the unique attributes of a hydrogel. The independent chemical and geometric tunability of our gel scaffold offers flexibility in terms of capture, partitioning, and release of biomolecules. Furthermore, the solid gel support establishes aqueous compartments with predefined volumes, containers with minimal biomolecule transport limitations, a mostly aqueous environment (>80% v/v liquid), and no need for surfactants. The rational design and flexibility of this approach will allow it to be applied to other biomolecule and cellular assays.

## ASSOCIATED CONTENT

### Supporting Information

Additional supporting equations, figures, and tables are available as noted in text. This material is available free of charge via the Internet at http://pubs.acs.org.

## AUTHOR INFORMATION

### Corresponding Author

*E-mail: pdoyle@mit.edu.

### Notes

The authors declare no competing financial interest.

## ACKNOWLEDGMENTS

We acknowledge funding from the NIH Center for Future Technologies in Cancer Care U54-EB-015403-01, NIH T32 GM08334 Interdepartmental Biotechnology Training Grant, and NSF Grant CMMI-1120724. We also thank Gaelle Le Goff and Hyewon Lee for useful discussions and for providing comments on the manuscript.

## REFERENCES

(1) Giljohann, D. A.; Mirkin, C. A. *Nature* **2009**, *462*, 461−464.
(2) Engvall, E.; Perlmann, P. *Immunochemistry* **1971**, *8*, 871−&.
(3) Kindt, T. J.; Goldsby, R. A.; Osborne, B. A.; Kuby, J. *Kuby immunology*, 6th ed.; W.H. Freeman: New York, 2007.
(4) Wild, D. *The immunoassay handbook: theory and applications of ligand binding, ELISA, and related techniques*, 4th ed.; Elsevier: Oxford, 2013;
(5) Rissin, D. M.; Kan, C. W.; Campbell, T. G.; Howes, S. C.; Fournier, D. R.; Song, L.; Piech, T.; Patel, P. P.; Chang, L.; Rivnak, A. J.; Ferrel, E. P.; Randall, J. D.; Provuncher, G. K.; Walt, D. R.; Duffy, D. C. *Nat. Biotechnol.* **2010**, *28*, 595−599.
(6) Rissin, D. M.; Fournier, D. R.; Piech, T.; Kan, C. W.; Campbell, T. G.; Song, L.; Chang, L.; Rivnak, A. J.; Patel, P. P.; Provuncher, G. K.; Ferrell, E. P.; Howes, S. C.; Pink, B. A.; Minnehan, K. A.; Wilson, D. H.; Duffy, D. C. *Anal. Chem.* **2011**, *83*, 2279−2285.
(7) Kan, C. W.; Rivnak, A. J.; Campbell, T. G.; Piech, T.; Rissin, D. M.; Mosl, M.; Peterca, A.; Niederberger, H.-P.; Minnehan, K. A.; Patel, P. P.; Ferrell, E. P.; Meyer, R. E.; Chang, L.; Wilson, D. H.; Fournier, D. R.; Duffy, D. C. *Lab Chip* **2012**, *12*, 977−985.
(8) Sakakihara, S.; Araki, S.; Iino, R.; Noji, H. *Lab Chip* **2010**, *10*, 3355−3362.
(9) Kim, S. H.; Iwai, S.; Araki, S.; Sakakihara, S.; Iino, R.; Noji, H. *Lab Chip* **2012**, *12*, 4986−4991.
(10) Song, H.; Chen, D. L.; Ismagilov, R. F. *Angew. Chem.* **2006**, *45*, 7336−56.
(11) Theberge, A. B.; Courtois, F.; Schaerli, Y.; Fischlechner, M.; Abell, C.; Hollfelder, F.; Huck, W. *Angew. Chem.* **2010**, *49*, 5846−5868.
(12) Zhang, H.; Nie, S.; Etson, C. M.; Wang, R. M.; Walt, D. R. *Lab Chip* **2012**, *12*, 2229−2239.
(13) Song, H.; Tice, J. D.; Ismagilov, R. F. *Angew. Chem.* **2003**, *42*, 768−772.
(14) Schmitz, C. H. J.; Rowat, A. C.; Koster, S.; Weitz, D. A. *Lab Chip* **2009**, *9*, 44−49.
(15) Baret, J. C.; Miller, O. J.; Taly, V.; Ryckelynck, M.; El-Harrak, A.; Frenz, L.; Rick, C.; Samuels, M. L.; Hutchison, J. B.; Agresti, J. J.; Link, D. R.; Weitz, D. A.; Griffiths, A. D. *Lab Chip* **2009**, *9*, 1850−1858.
(16) Joensson, H. N.; Samuels, M. L.; Brouzes, E. R.; Medkova, M.; Uhlen, M.; Link, D. R.; Andersson-Svahn, H. *Angew. Chem.* **2009**, *48*, 2518−2521.
(17) Tewhey, R.; Warner, J. B.; Nakano, M.; Libby, B.; Medkova, M.; David, P. H.; Kotsopoulos, S. K.; Samuels, M. L.; Hutchison, J. B.; Larson, J. W.; Topol, E. J.; Weiner, M. P.; Harismendy, O.; Olson, J.; Link, D. R.; Frazer, K. A. *Nat. Biotechnol.* **2009**, *27*, 1025−U94.
(18) Ogunniyi, A. O.; Story, C. M.; Papa, E.; Guillen, E.; Love, J. C. *Nat. Protoc.* **2009**, *4*, 767−782.
(19) Beer, N. R.; Hindson, B. J.; Wheeler, E. K.; Hall, S. B.; Rose, K. A.; Kennedy, I. M.; Colston, B. W. *Anal. Chem.* **2007**, *79*, 8471−8475.
(20) Love, J. C.; Wolfe, D. B.; Jacobs, H. O.; Whitesides, G. M. *Langmuir* **2001**, *17*, 6005−6012.
(21) Liu, J.; Gao, D.; Li, H.-F.; Lin, J.-M. *Lab Chip* **2009**, *9*, 1301−1305.
(22) Pregibon, D. C.; Toner, M.; Doyle, P. S. *Langmuir* **2006**, *22*, 5122−5128.
(23) Beebe, D. J.; Moore, J. S.; Bauer, J. M.; Yu, Q.; Liu, R. H.; Devadoss, C.; Jo, B. H. *Nature* **2000**, *404*, 588−+.
(24) Arenkov, P.; Kukhtin, A.; Gemmell, A.; Voloshchuk, S.; Chupeeva, V.; Mirzabekov, A. *Anal. Biochem.* **2000**, *278*, 123−131.
(25) Fotin, A. V.; Drobyshev, A. L.; Proudnikov, D. Y.; Perov, A. N.; Mirzabekov, A. D. *Nucleic Acids Res.* **1998**, *26*, 1515−1521.
(26) Proudnikov, D.; Timofeev, E.; Mirzabekov, A. *Anal. Biochem.* **1998**, *259*, 34−41.
(27) Heo, J.; Crooks, R. M. *Anal. Chem.* **2005**, *77*, 6843−6851.
(28) Koh, W. G.; Pishko, M. *Sens. Actuators, B* **2005**, *106*, 335−342.
(29) Lee, A. G.; Arena, C. P.; Beebe, D. J.; Palecek, S. P. *Biomacromolecules* **2010**, *11*, 3316−3324.
(30) Lee, A. G.; Beebe, D. J.; Palecek, S. P. *Biomed. Microdevices* **2012**, *14*, 247−257.
(31) Li, H. Y.; Leulmi, R. F.; Juncker, D. *Lab Chip* **2011**, *11*, 528−534.
(32) Ikami, M.; Kawakami, A.; Kakuta, M.; Okamoto, Y.; Kaji, N.; Tokeshi, M.; Baba, Y. *Lab Chip* **2010**, *10*, 3335−3340.
(33) Manage, D. P.; Lauzon, J.; Atrazhev, A.; Morrissey, Y. C.; Edwards, A. L.; Stickel, A. J.; Crabtree, H. J.; Pabbaraju, K.; Zahariadis, G.; Yanow, S. K.; Pilarski, L. M. *Lab Chip* **2012**, *12*, 1664−1671.
(34) Manage, D. P.; Chui, L. D.; Pilarski, L. M. *Microfluid. Nanofluid.* **2013**, *14*, 731−741.

(35) Atrazhev, A.; Manage, D. P.; Stickel, A. J.; Crabtree, H. J.; Pilarski, L. M.; Acker, J. P. *Anal. Chem.* **2010**, *82*, 8079−8087.
(36) Rubina, A. Y.; Kolchinsky, A.; Makarov, A. A.; Zasedatelev, A. S. *Proteomics* **2008**, *8*, 817−831.
(37) Choi, N. W.; Kim, J.; Chapin, S. C.; Duong, T.; Donohue, E.; Pandey, P.; Broom, W.; Hill, W. A.; Doyle, P. S. *Anal. Chem.* **2012**, *84*, 9370−9378.
(38) Pregibon, D. C.; Doyle, P. S. *Anal. Chem.* **2009**, *81*, 4873−4881.
(39) Appleyard, D. C.; Chapin, S. C.; Srinivas, R. L.; Doyle, P. S. *Nat. Protoc.* **2011**, *6*, 1761−1774.
(40) Chapin, S. C.; Appleyard, D. C.; Pregibon, D. C.; Doyle, P. S. *Angew. Chem.* **2011**, *50*, 2289−2293.
(41) Bong, K. W.; Chapin, S. C.; Pregibon, D. C.; Baah, D.; Floyd-Smith, T. M.; Doyle, P. S. *Lab Chip* **2011**, *11*, 743−747.
(42) Gorris, H. H.; Walt, D. R. *J. Am. Chem. Soc.* **2009**, *131*, 6277−6282.
(43) Piwonski, H. M.; Goomanovsky, M.; Bensimon, D.; Horovitz, A.; Haran, G. *Proc. Natl. Acad. Sci. U. S. A.* **2012**, *109*, E1437−E1443.
(44) Chang, L.; Rissin, D. M.; Fournier, D. R.; Piech, T.; Patel, P. P.; Wilson, D. H.; Duffy, D. C. *J. Immunol. Methods* **2012**, *378*, 102−115.
(45) Huang, Z. J. *Biochemistry* **1991**, *30*, 8535−8540.
(46) Lee, W.; Choi, D.; Kim, J.-H.; Koh, W.-G. *Biomed. Microdevices* **2008**, *10*, 813−822.
(47) Pregibon, D. C.; Toner, M.; Doyle, P. S. *Science* **2007**, *315*, 1393−1396.
(48) Lewis, C. L.; Choi, C. H.; Lin, Y.; Lee, C. S.; Yi, H. *Anal. Chem.* **2010**, *82*, 5851−5858.